A “Click” Reaction to Engineer MoS2 Field-Effect Transistors with Low Contact Resistance

Jialei Miao, Linlu Wu, Zheng Bian, Qinghai Zhu, Tianjiao Zhang, Xin Pan, Jiayang Hu, Wei Xu, Yeliang Wang, Yang Xu, et al.

A "Click" Reaction to Engineer MoS_2 Field-Effect Transistors with Low Contact Resistance

*Jialei Miao,[1,2,#] Linlu Wu,[3,#] Zheng Bian,[1] Qinghai Zhu, [1] Tianjiao Zhang, [1] Xin Pan, [1] Jiayang Hu, [1] Wei Xu,[4] Yeliang Wang,[5] Yang Xu, [1] Bin Yu, [1] Wei Ji, [3] Xiaowei Zhang, *[,2] Jingsi Qiao,*[,5] Paolo Samorì,*[,6] Yuda Zhao*[,1,7]*

[1] School of Micro-Nano Electronics, Hangzhou Global Scientific and Technological Innovation Centre, Zhejiang University, 38 Zheda Road, Hangzhou, 310027, China.

[2] Department of Electrical Engineering and Computer Science, Ningbo University, Ningbo, 315211, China.

[3] Beijing Key Laboratory of Optoelectronic Functional Materials & Micro-Nano Devices, Department of Physics, Renmin University of China, Beijing 100872, China

[4] Research Centre for Humanoid Sensing, Zhejiang Lab, Hangzhou, 311121, China.

[5] MIIT Key Laboratory for Low-Dimensional Quantum Structure and Devices, School of Integrated Circuits and Electronics, Beijing Institute of Technology, Beijing 100081, China

[6] University of Strasbourg, CNRS, ISIS UMR 7006, 8 allée Gaspard Monge, F-67000 Strasbourg, France

[7] Key Laboratory of Optoelectronic Chemical Materials and Devices of Ministry of Education, Jianghan University, Wuhan 430056, China

KEY WORDS: Two-dimensional materials, covalent functionalization, carrier doping, contact resistance, thermal stability

Abstract: Two-dimensional (2D) materials with the atomically thin thickness have attracted great interest in the post-Moore's Law era because of their tremendous potential to continue transistor downscaling and offered advances in device performance at the atomic limit. However, the metal-semiconductor contact is the bottleneck in field-effect transistors (FETs) integrating 2D semiconductors as channel materials. A robust and tunable doping method at the source and drain region of 2D transistors to minimize the contact resistance is highly sought after. Here we report a stable carrier doping method via the mild covalent grafting of maleimides on the surface of 2D transition metal dichalcogenides. The chemisorbed interaction contributes to the efficient carrier doping without degrading the high-performance carrier transport. Density functional theory results further illustrate that the molecular functionalization leads to the mild hybridization and the negligible impact on the conduction bands of monolayer MoS_2, avoiding the random scattering from the dopants. Differently from reported molecular treatments, our strategy displays high thermal stability (above 300 °C) and it is compatible with micro/nano processing technology. The contact

resistance of MoS_2 FETs can be greatly reduced by ~12 times after molecular functionalization. The Schottky barrier of 44 meV is achieved on monolayer MoS_2 FETs, demonstrating efficient charge injection between metal and 2D semiconductor. The mild covalent functionalization of molecules on 2D semiconductors represents a powerful strategy to perform the carrier doping and the device optimization.

Two-dimensional (2D) materials maintain a high carrier mobility down to the sub-1 nm thickness and show high immunity to the short-channel effect, displaying the potential to ultimately scale down the transistor dimensions.[1-3] However, the charge transport in field-effect transistors (FETs) based on 2D semiconductor channels has been hampered by extrinsic factors, such as the high contact resistance, interface scattering and defects.[1-3] In the meanwhile, a strong Fermi level pinning effect is observed between bulk metals and 2D semiconductors, making the realization of Ohmic contact challenging.[4] It is the prerequisite to achieve the efficient injection of charge carrier from the contacts to the 2D semiconductor channel to achieve the high-performance operation, especially in short-channel and high-frequency transistors.

In traditional silicon-based technology, degenerate doping by ion implantation can effectively minimize the contact resistance and reduce the Schottky barrier to enhance the carrier injection. Although the ion implantation is not compatible with ultrathin 2D materials due to the severe formation of defects, the degenerate doping at the contact region is an effective methodology to perform contact engineering in 2D FETs. Chhowalla *et al.* reported the use of phase-engineered metallic MoS_2 as the contact to achieve an ultralow contact resistance of 200-300 $\Omega \cdot \mu m$ at zero gate bias.[4] Recently, semimetallic bismuth was used to form high-quality Ohmic contact with monolayer MoS_2 due to the suppression of the metal-induced gap states and the degenerate doping at the contact region.[5] Molecular functionalization of 2D FETs with decanethiol,[6] benzyl viologen,[7, 8] NO_2,[9] and tungsten oxyselenide[10] at the contact regions have been successfully demonstrated to improve the charge injection. However, the thermal

stability is the bottleneck of these methods and the molecular functionalization methods also exhibit the poor complementary metal-oxide-semiconductor (CMOS) compatibility. The covalent functionalization of a 2D semiconductor channel with molecules show the advantages of the high thermal stability, but degrade the electrical transport properties because the highly ordered crystalline structure of 2D semiconductors would be interrupted by the molecules. It is highly desirable to develop a mild covalent functionalization method to simultaneously achieve the stable carrier doping of 2D semiconductors, preserve the excellent electrical transport properties of 2D layers, display high thermal stability, and be compatible with CMOS process.

In this work, we propose a powerful strategy to realize efficient n-type doping on 2D transition metal disulfide MoS_2 via a mild "click" reaction. The sulfur atoms with soft nucleophilicity react with maleimide via Michael addition to achieve the covalent functionalization.[11] The molecular functionalization at the channel region results in the increased electron density of MoS_2 by 2.18×10^{12} cm^{-2}. The material and device characterizations demonstrate the successful n-type doping of the MoS_2 layer. The functionalized MoS_2 layers are compatible with micro/nano fabrication process and the fabricated transistors show high thermal stability at over 300 °C. Furthermore, by using a micropatterning process, the contact regions between metal and MoS_2 are selectively doped via the mild "click" reaction. The average contact resistance of MoS_2 transistors is as low as 4.4 kΩ·μm, which is 12 times smaller than pristine devices. The Schottky barrier has been reduced to 44 meV in monolayer MoS_2 transistors with Au electrodes. The field-effect mobility of monolayer and three-layer MoS_2 FETs reaches values as

high as 57 and 61 $cm^2V^{-1}s^{-1}$, respectively. Density functional theory results indicate that electron transport of MoS_2 is dominated by the *d* orbitals of Mo atoms, which have not been interfered by the C-S bonds of molecular functionalization. The mild covalent functionalization provides a feasible pathway to optimize the performance of 2D transistors, which is compatible with back-end-of-line (BEOL) integration in large-scale production.

Results and discussion

Thiol-maleimide "click" reaction via Michael addition is an efficient approach to achieve surface modification in polymers and biomaterials. In 2019, Pérez *et al.* demonstrated the successful covalent functionalization of liquid-phase exfoliated transition metal disulfides (TMDs) with maleimide via a "click" reaction,[11] showing the potential to perform covalent functionalization of 2D semiconductors under mild conditions. The MoS_2 flakes in our work were mechanically exfoliated from bulk MoS_2 crystals and transferred to the SiO_2/Si substrate (oxide thickness 285 nm). Figure 1a schematically illustrates the covalent functionalization process and the experimental details can be found in the Method section. Generally, the MoS_2 samples were soaked overnight in the solution comprised of *N*-benzylmaleimide, acetonitrile, and triethylamine at room temperature under a N_2 atmosphere. X-ray photoelectron spectroscopy (XPS) was employed to characterize the covalent C-N bonding in MoS_2 after the functionalization with *N*-benzylmaleimide (abbreviated as Nbm-MoS_2). Compared with pristine MoS_2, a characteristic peak for N 1s appears as shown in Figure

1b, which can be unambiguously assigned to the maleimide fragment. After 350 °C annealing, N 1s peak is greatly weakened (Figure S1) due to the desorption of covalently attached materials, which is consistent with the thermogravimetric analysis of the Nbm-MoS_2 samples as reported by Pérez *et al.*[11]

Raman spectra of Nbm-MoS_2 and pristine MoS_2 display typical A_{1g} and E^1_{2g} Raman peaks in Figure S2a. The crystal structure of MoS_2 has been well preserved. Photoluminescence (PL) spectroscopy is a reliable method to characterize the doping of layered TMDs.[12] Figure 1c shows the PL spectra of Nbm-MoS_2 and pristine MoS_2 with A and B exciton peaks. The A exciton peak of monolayer MoS_2 consists of a neutral exciton peak ($E(X) \approx 1.88$ eV) and a negatively charged trion peak ($E(X^-) \approx 1.84$ eV),[13] and the spectra weight is an indicator of the MoS_2 electron density.[14] Our results show that the weight of the neutral exciton peak decreased from 41.7 % to 6.3 %, and the trion peak weight increased from 52.7 % to 59.8 %, demonstrating the increase of electron density in MoS_2. The emergence of a new peak (X_1) at 1.60 eV in Nbm-MoS_2 demonstrates the existence of mid-gap states and the hybridization between MoS_2 and *N*-benzylmaleimide. The XPS spectra of Mo and S core levels for pristine and Nbm-MoS_2 are shown in Figure 1d and S2b. The Mo 3d peaks and S 2p peaks show blue shift after Nbm functionalization, demonstrating the electron doping. The material characterization results prove the efficient n-type doping of MoS_2 after molecular functionalization.

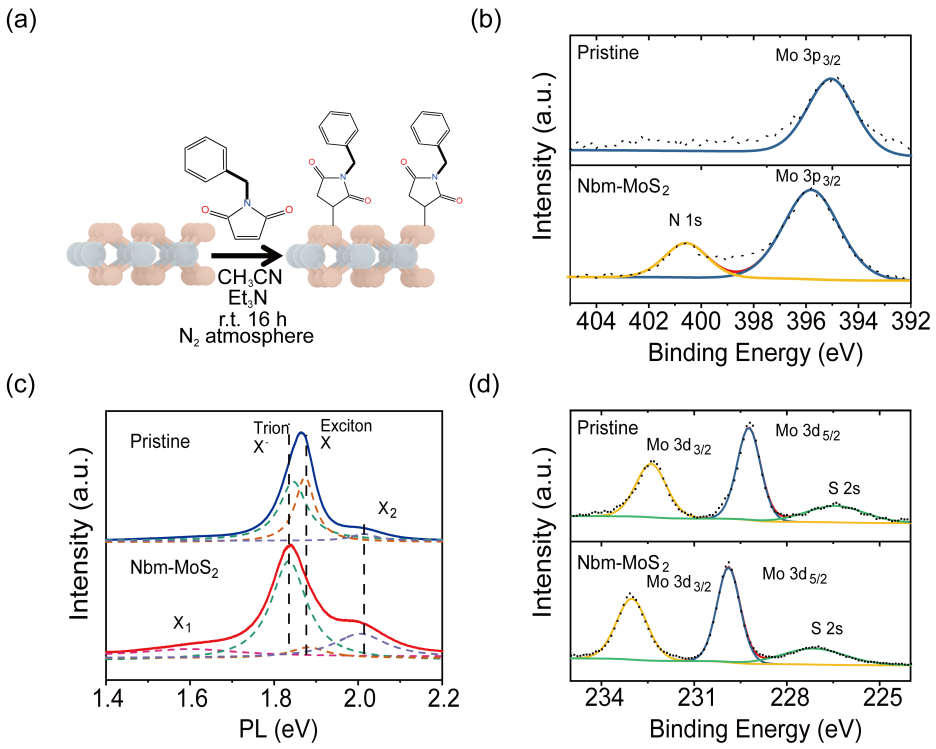

Figure 1. Spectroscopic characterizations of the functionalized MoS_2 (Nbm-MoS_2). (a) Schematic of the mild "click" reaction between MoS_2 and N-benzylmaleimide. (b) XPS spectra of N 1s core level for pristine MoS_2 and Nbm-MoS_2. (c) Photoluminescence (PL) spectra of the pristine MoS_2 and Nbm-MoS_2. (d) XPS spectra of Mo core level for pristine MoS_2 and Nbm-MoS_2.

The preservation of excellent electrical transport properties of the functionalized MoS_2 samples is crucial to their applications in advanced electronic devices. To investigate the electrical properties of Nbm-MoS_2 FETs, the back-gate top-contact MoS_2 FETs were fabricated on hexagonal boron nitride (h-BN)/SiO_2 bilayer dielectric substrate with 40-nm-thick Au top electrodes, and then the exposed MoS_2 channel was functionalized with *N*-benzylmaleimide (Figure 2a). The device fabrication details are

provided in the Method section. The h-BN is used as an interfacial dielectric layer to improve the quality of the MoS_2/dielectric interface because the carriers in the atomically thin MoS_2 can be dramatically scattered by the defects and surface states of SiO_2.[15, 16] Figure 2b shows the transfer and output characteristics of the monolayer MoS_2 FETs before and after the molecular functionalization (0.5 mmol *N*-benzylmaleimide) in the channel region. Compared with pristine MoS_2 FETs, the Nbm-MoS_2 FETs exhibit improved on-state current, comparable off-state current, increased I_{on}/I_{off} ratio (over 10^5), and the negative shift of the threshold voltage (ΔV_{th} = 29 V). It suggests that *N*-benzylmaleimide can induce the n-doping in MoS_2 which is evidenced by an electron density change (Δn) of 2.18×10^{12} cm^{-2}. Taking advantage of the mild covalent functionalization, the field-effect mobility increases from 33 $cm^2V^{-1}s^{-1}$ (pristine) to 59 $cm^2V^{-1}s^{-1}$ (Nbm-MoS_2). The increased electron density of monolayer MoS_2 greatly screen the scattering and improve the carrier mobility. The hysteresis of transfer curves of Nbm-MoS_2 FET can reflect the MoS_2/molecule interface quality. Compared with pristine device, the Nbm-MoS_2 FET (0.1 mmol Nbm) displays a small hysteresis as shown in Figure S3a, demonstrating the limited influence of functionalized molecules on the electron transport of MoS_2 FETs. The concentration of *N*-benzylmaleimide determines the functional ratio and the charge density in MoS_2. We further explored the relation between the functionalization ratio and the charge transport in Nbm-MoS_2 FETs as shown in Figure S4 and obtained the optimized molecular concentration. In devices fabricated on SiO_2/Si substrate, the monolayer Nbm-MoS_2

FETs show weak electrostatic gate modulation and high off-state current (Figure S5), demonstrating the degenerate doping of MoS_2 by *N*-benzylmaleimide molecules.

One important merit of the covalent functionalization is the high thermal stability, which is also a significant prerequisite for large-scale production and BEOL integration. In experiment, the Nbm-MoS_2 FETs were annealed at several temperatures from 200 ℃ to 350 ℃ to show the thermal stability. The thermal annealing was performed in a tube furnace at low pressure with 100 sccm H_2/Ar (10%/90%) flow. After the annealing treatment at 200 ℃, 250 ℃, and 300℃, the device preserved the excellent electrical transport behavior (Figure 2c, 2d and Figure S6), further demonstrating the formation of covalent bonds between MoS_2 and *N*-benzylmaleimide, instead of physisorption (boiling point of *N*-benzylmaleimide is 177 ℃). After 350 ℃ annealing, the electrical transport performance dramatically degraded due to the desorption of covalently attached materials and the figures of merit of Nbm-MoS_2 FETs were even worse than the performance before thermal annealing. The disappearance of N 1s peak in the XPS spectra of Nbm-MoS_2 after 350 ℃ annealing (Figure S1) provides evidence for the desorption of Nbm fragments. The thermal stability tests show that the mild covalent bonding of *N*-benzylmaleimide on monolayer MoS_2 surface can simultaneously improve the electrical transport properties and display high thermal stability. In comparison, conventional doping strategies by physisorbed molecules mostly show poor thermal stability and cannot endure a high-temperature process.[17] Therefore, our method exhibits a valuable advantage in large-scale production and BEOL integration.

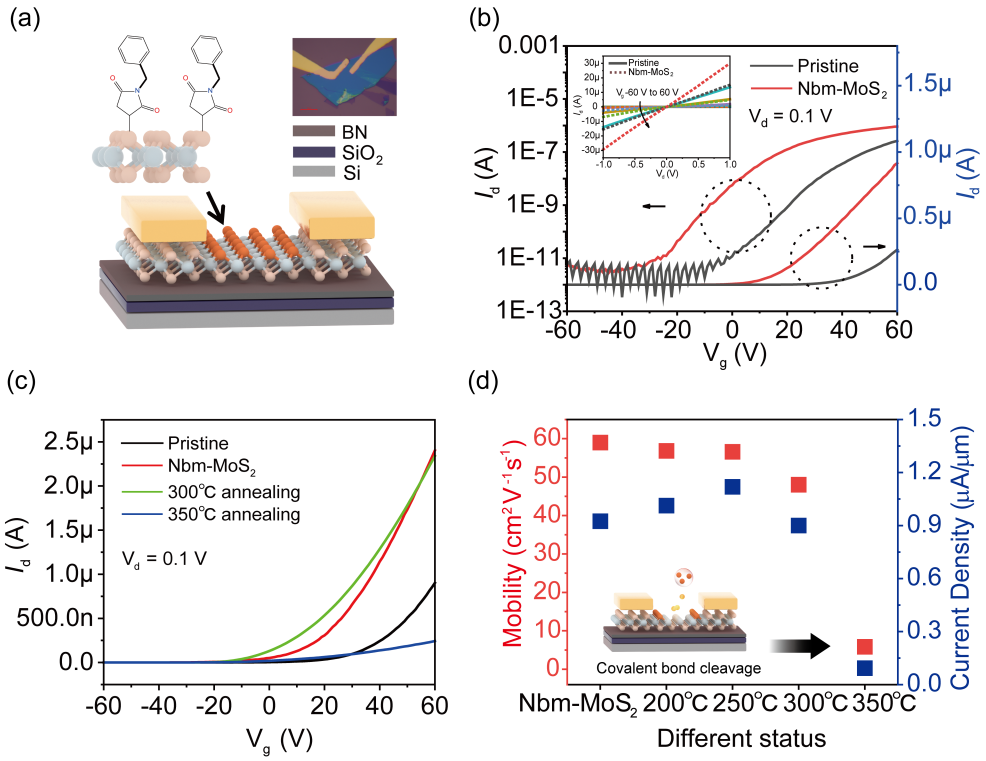

Figure 2. Electrical characterizations of monolayer Nbm-MoS_2 FETs. (a) Schematic of the Nbm-MoS_2 FET with the channel region functionalized with *N*-benzylmaleimide. (b) Transfer curves of the pristine and Nbm-MoS_2 FET. Inset shows the output curves. (c) Transfer curves of the pristine MoS_2 FET, Nbm-MoS_2 FET, and Nbm-MoS_2 FETs after 300 ℃ and 350 ℃ annealing, respectively. (d) Mobility and current density are extracted from Figure 2c and Figure S6. The dramatic performance degradation after 350 ℃ annealing indicates the cleavage of covalent bonds.

In pristine samples, the sulfur atom in MoS_2 is covalently bound to three Mo atoms. The “click” reaction with maleimide induces the formation of hypervalent S species with covalent bonds to three Mo atoms and one C atom. Finally, the negative formal charge on the S atoms would facilitate the electron extraction and hence the electronic properties of TMDs can be efficiently modulated via the covalent functionalization. To

explore the in-depth mechanism of the excellent electrical transport of Nbm-MoS_2, we further performed first-principles DFT calculations to study the electronic structure of Nbm-MoS_2. The most energetically favored structure of Nbm-MoS_2 is shown in Figure 3a (see Figure S7 for more discussions). The chemical absorption manifests as covalent C-S bonding and the hydrogen atom is transferred to the adjacent C atoms. To explore the influence of the covalent functionalization of MoS_2 with *N*-benzylmaleimide, we calculated the decomposed atomic/orbital band structure of Nbm-MoS_2 (Figure 3b). A mid-gap state, identified as the highest occupied molecule orbital (HOMO) of the *N*-benzylmaleimide, emerged in the bandgap of pristine MoS_2. The norm of the wavefunctions for the localized mid-gap state, Nbm-HOMO labeled in Figure 3b, were visualized in Figure 3c. As shown in Figure S8, the states around valence bands maximum (VB1 and VB2) of pristine MoS_2 are contributed by *p* orbital of S atoms. In comparison, the six valence bands below the band of Nbm-HOMO in Nbm-MoS_2 present C-S bonding (Figure S9), which has a negative effect on the hole transport of MoS_2. However, the conduction band minimum states of MoS_2 are mainly comprised of Mo dz^2 orbital (CB1 of Figure S8b) and the electron transport of MoS_2 has not been interfered with the covalently functionalized molecules on MoS_2 (Figure 3d and 3e). Actually, as the projected bands on the orbital of Nbm molecule shown in the red dots of Figure 3b, the lowest unoccupied orbital (LUMO) of the *N*-benzylmaleimide arises at ~3 eV higher than the conduction band minimum (CBM) band of Nbm-MoS_2, which have negligible influence on the electron transport of MoS_2. Overall, the mild covalent functionalization of MoS_2 with *N*-benzylmaleimide can increase the electron density,

preserve the intrinsic electron transport properties without any degradation, and suppress the impurity scattering from external environment. These results demonstrate the mild covalent functionalization is a powerful strategy to engineer the properties of MoS_2 and optimize the device performance.

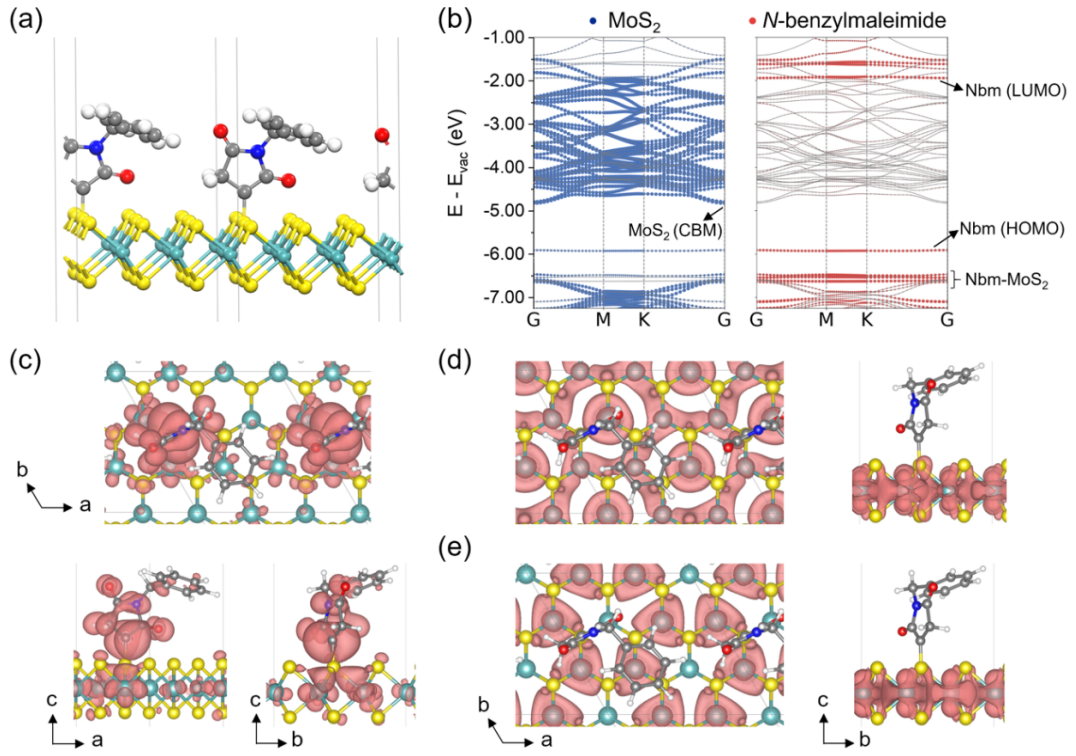

Figure 3. Geometric and Electronic band structure of Nbm-MoS_2. (a) Atomic configuration of Nbm-MoS_2. (b) Decomposed atomic band structure of Nbm-MoS_2. Blue and red dots represent the bands decomposed on the orbitals of MoS_2 (left panel) and the N-benzylmaleimide molecules (right panel), respectively. The highest occupied molecular orbital (HOMO) and the lowest unoccupied molecular orbital (LUMO) of the N-benzylmaleimide, the highest valence bands and the conduction band minimum (CBM) of MoS_2 are labeled as Nbm (HOMO), Nbm (LUMO), Nbm-MoS_2 and MoS_2-(CBM), respectively. (c) Spatial structure of wavefunction norms for the Nbm-HOMO

states labelled in b at the G point in the *ab*, *ac* and *bc* planes, respectively. (d-e) Spatial structure of wavefunction norms for the two-fold degenerated MoS_2-CBM states at the G point. Isosurface level of (c)-(e) is 1.0×10^{-4} *e*/Bohr^3.

As the covalent functionalization method can effectively modulate the electronic properties and even realize degenerate doping of MoS_2, it is interesting to apply this strategy to decrease the contact resistance of MoS_2 FETs. In MoS_2 transistors, the existence of Schottky barriers at the metal-semiconductor interface fundamentally leads to high contact resistance, which follows the Mott-Schottky rule.[18] The degenerate doping of 2D semiconductors at the contact region will effectively decrease the Schottky barrier and reduce the contact resistance. The schematic of the device structure with contact engineering is shown in Figure 4a and the MoS_2 transistors were selectively doped at the contact region by the *N*-benzylmaleimide molecules (abbreviated as Nbm-ct-MoS_2 FETs). To investigate the carrier injection at the semiconductor/metal junction in Nbm-ct-MoS_2 FETs, the transfer and output curves at different temperatures were measured in a cryogenic probe station. For the sake of comparison, the drain current is normalized by channel length and width. The transfer curves of monolayer MoS_2 FET are shown in Figure 4b. Owing to the improved charge injection at the semiconductor/metal junction, the electrical transport performance of monolayer Nbm-ct-MoS_2 FET has been significantly enhanced. The field-effect mobility of monolayer MoS_2 FETs was increased from 20 $cm^2V^{-1}s^{-1}$ to 57 $cm^2V^{-1}s^{-1}$ at room temperature and the normalized drain current was boosted from 0.9 μA to 3.1 μA

at V_d = 0.1 V. The pristine MoS_2 and Nbm-ct-MoS_2 FETs were fabricated on the same flake to avoid device variation (Figure S10) and the Nbm-ct-MoS_2 FET displayed improved performance, undoubtedly proving the positive effect of Nbm. We further employed the transfer length method (TLM) to characterize the contact resistance.[19] Figure 4c plots the normalized resistance as a function of the channel length and the contact resistance is extracted from the y-intercept of the fitted linear line. With the molecular doping at the contact region, the device of three-layer Nbm-ct-MoS_2 FET reaches a contact resistance (R_c) as low as 3.7 kΩ·μm. Raman and AFM characterizations in Figure S11 confirm the uniformity and the thickness of the channel layer. Compared with the average contact resistance of pristine MoS_2 FET of 52.9 kΩ·μm (Figure S12), the average contact resistance of Nbm-ct-MoS_2 FETs of 4.4 kΩ·μm (Figure S13) is greatly reduced by 12 times. The output curves of the Nbm-ct-MoS_2 FET and pristine MoS_2 FET at 150 K are displayed in Figure 4d. The excellent Ohmic contact in the Nbm-ct-MoS_2 FET contributes to the linear output curves even at low temperature, while the pristine MoS_2 FET with Schottky contact shows nonlinear output curves. Owing to the high-quality contact and dielectric interface in Nbm-ct-MoS_2 FET, the hysteresis is nearly zero on monolayer Nbm-ct-MoS_2 FETs as shown in Figure S3b. A Nbm-ct-MoS_2 FET with a 500 nm channel length was fabricated and the device displayed a high current density of 83.4 μA/μm at V_d = 1V as shown in Figure S14. These results demonstrate that the molecular functionalization at the contact region effectively reduces the contact resistance and improves the charge injection between 2D materials and the metal contact. We would like to point out that this high-

quality molecular functionalization strategy is compatible with the micro/nano fabrication process, because the functionalization procedure is carried out before the patterning and the deposition of source/drain electrodes.

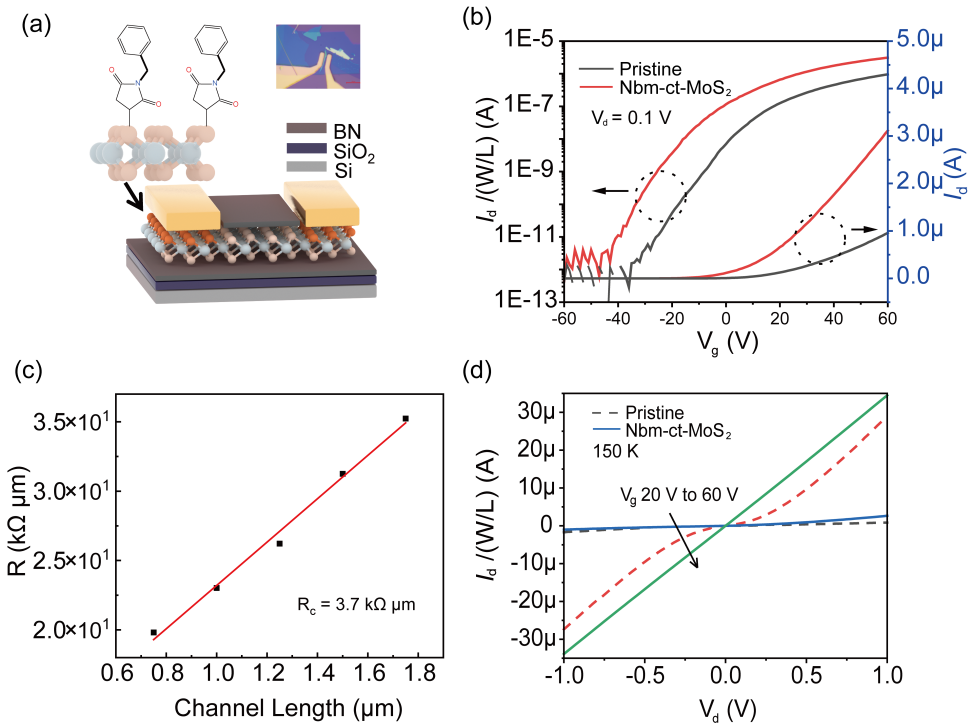

Figure 4. Contact engineering of MoS_2 FETs by covalent functionalization. (a) Schematic of the MoS_2 FET with *N*-benzylmaleimide functionalized at the contact region (Nbm-ct-MoS_2 FET). (b) Transfer curves of monolayer Nbm-ct-MoS_2 FET and pristine MoS_2 FET. (c) The normalized resistance of three-layer Nbm-ct-MoS_2 FETs at V_g = 60 V along with the channel lengths. Contact resistance has been extracted from the fitted linear line by the transfer length method (TLM). (d) Output curves of the Nbm-ct-MoS_2 FET and pristine MoS_2 FET at 150 K.

Systematic temperature-dependent electrical transport characterizations are performed on pristine MoS_2 FETs and Nbm-ct-MoS_2 FETs. In pristine monolayer MoS_2 FET (Figure 5a), the drain current shows a dramatic drop with the decreasing temperature, owing to the reduction of thermionic emission current at contact. Due to the two-probe measurement configuration, the MoS_2/metal contact greatly affects the temperature-dependent charge transport. Monolayer and three-layer Nbm-ct-MoS_2 FETs in Figure 5b and 5c only exhibit a slight decrease of the drain current when temperature reduces from 300 K to 150 K. In the meanwhile, a carrier-density dependent metal-insulator transition (MIT) has been observed in Nbm-ct-MoS_2 FETs,[20] indicating the formation of good MoS_2/metal contact to achieve the efficient charge injection even at low temperature.

The temperature-dependent field-effect mobilities of the pristine monolayer, monolayer Nbm-ct-MoS_2, and three-layer Nbm-ct-MoS_2 FETs have been plotted in Figure 5d. Within the temperature range from 300 K to 200 K, phonon scattering is the dominant mechanism to affect the electron mobility of MoS_2 and the mobility is expected to follow a $\mu \sim T^{-\gamma}$ temperature dependence. The value of γ in pristine monolayer MoS_2 FETs is nearly zero, which proves that the contact resistance is dominant factor rather than phonon scattering. In monolayer and three-layer Nbm-ct-MoS_2 FETs, the value of γ is 0.73 and 1.02, respectively. These numbers are approaching the theoretically predicted value for monolayer (1.52) and bulk (2.6) MoS_2 on the SiO_2/Si substrate.[21, 22] Previous works have demonstrated that both the top and the bottom dielectric environment can induce phonon screening or a change in the strength of electron-

phonon coupling, resulting in the decrease of the γ value.[23] Therefore, the slightly small γ value in Nbm-ct-MoS_2 FETs is perhaps due to the encapsulation of the MoS_2 channel by top and bottom h-BN layers. At low temperature below 200 K, the field-effect mobility of pristine monolayer MoS_2 FET greatly drops, and the mobility below 100 K becomes even smaller than 1 $cm^2V^{-1}s^{-1}$ because of the very limited charge injection from the MoS_2/metal contact. In contrast, monolayer and three-layer Nbm-ct-MoS_2 FETs maintain the high electron mobility until 25 K owing to the good MoS_2/metal contact and the weak impurity scattering.

The Schottky barrier can be extracted from the temperature-dependent electrical transport results. The drain current in the subthreshold region mainly depends on the thermionic emission current and the thermally-assisted tunneling current. When the gate voltage (V_g) is below the flat-band voltage (V_{FB}), the thermionic emission current dominates the current. When V_g is larger than V_{FB}, thermally-assisted tunneling current becomes dominant. When V_g equals V_{FB}, the Schottky barrier (Φ_B) can be extracted.[24-26] The Schottky barrier heights of pristine monolayer MoS_2 FET and monolayer Nbm-ct-MoS_2 FET are 174 meV and 44 meV (Figure 5e and 5f), respectively. The average Schottky barrier heights of pristine MoS_2 and Nbm-ct-MoS_2 FETs are shown in Figure S15 and S16, which is consistent with our representative devices. This confirms that the molecular functionalization at the contact region in Nbm-ct-MoS_2 FET can effectively modulate the work function of MoS_2 and reduce the Schottky barrier of MoS_2 FETs.

Several mechanisms contribute to the improved metal/MoS_2 contact in Nbm-ct-MoS_2 FETs. The functionalized molecule with the height of ~1 nm on MoS_2 surface can act as the tunneling layer between metal and MoS_2 to suppress the Fermi level pinning effect.[27, 28] The tunneling layer can be clearly seen in the cross-sectional high-resolution transmission electron microscopy (HR-TEM) image (Figure S17). The molecules can slightly increase the distance between metal and semiconductor and decouple the orbital overlap. The interfacial layer can also prevent the damage of MoS_2 surface from the high-energy metal atoms during the metal deposition process. Moreover, the theoretical band alignment between the CBM of Nbm-MoS_2 and the work function of Au shows the reduced Schottky barrier (Figure S18). Therefore, the increased electron density of Nbm-MoS_2 reduces the contact resistance and the Schottky barrier, facilitating the electron injection.

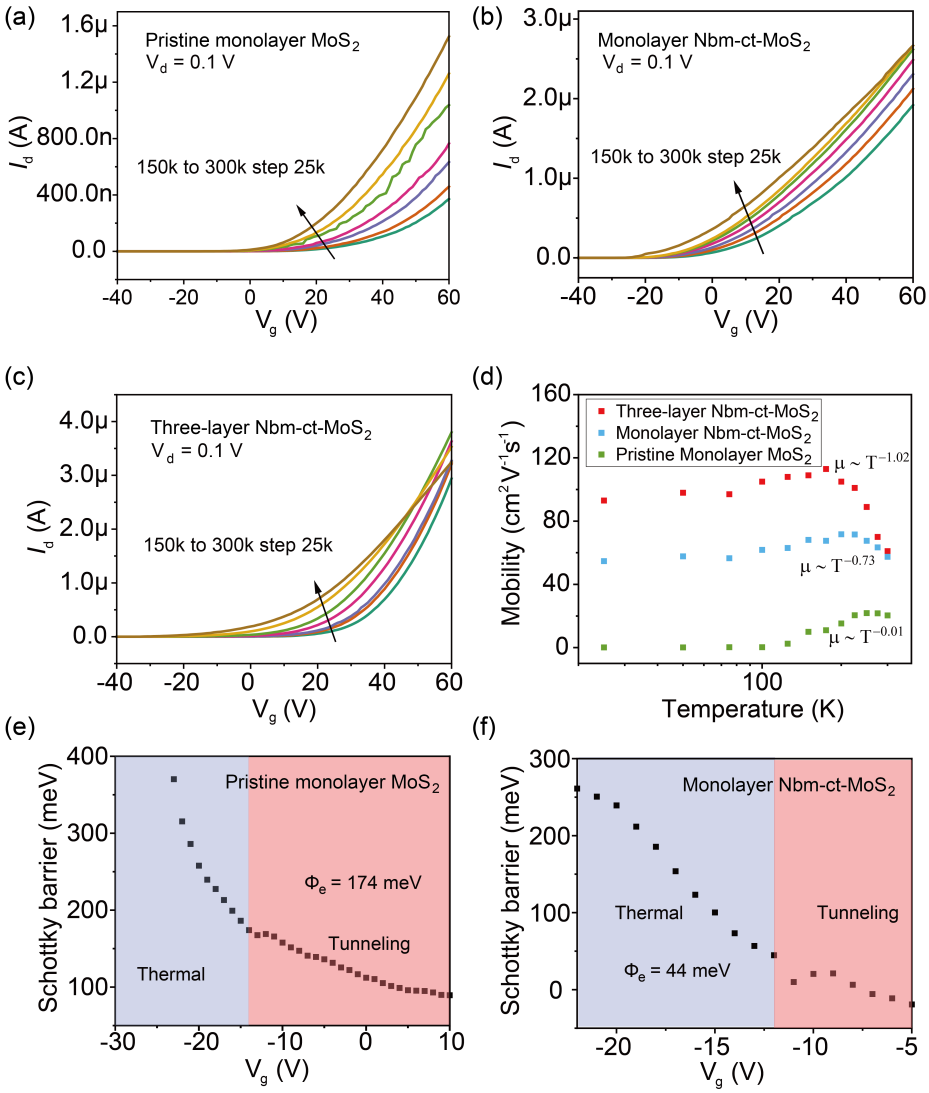

Figure 5. Temperature-dependent electrical characterizations of Nbm-ct-MoS_2 FETs. Temperature-dependent transfers curves of (a) pristine monolayer MoS_2 FETs, (b) monolayer Nbm-ct-MoS_2 FETs, and (c) three-layer Nbm-ct-MoS_2 FETs. (d) Temperature-dependent electron mobilities of pristine monolayer MoS_2 FETs, monolayer Nbm-ct-MoS_2 FETs, and three-layer Nbm-ct-MoS_2 FETs. Extraction of Schottky barriers from (e) pristine monolayer MoS_2 FETs and (f) monolayer Nbm-ct-MoS_2 FETs.

Conclusion

In conclusion, we dramatically reduced the contact resistance of MoS_2 FETs via the efficient n-type doping of MoS_2 at the contact region, realized by a mild covalent functionalization of MoS_2 with *N*-benzylmaleimide. This method can dope MoS_2 without interrupting the electron transport of MoS_2. Different from the traditional molecular doping methods, this strategy exhibits excellent thermal stability (above 300 °C), preserves the high-performance carrier transport behavior, and is compatible with micro/nano fabrication technology. The Nbm-ct-MoS_2 FET reached low contact resistance of 4.4 kΩ·μm by performing the selective doping at the contact region. The mild "click" reaction represents a versatile strategy to modulate the electronic properties of 2D semiconductors and optimize the electrical transport performance of 2D FETs.

Methods

Materials. Bulk molybdenum disulfide (MoS_2) crystals were purchased from Sixcarbon Technology. The Hexagonal Boron Nitride (h-BN) was purchased from HQ Graphene. The acetonitrile (ACN) was purchased from Sigma-Aldrich. The N-benzylmaleimide and triethylamine (Et_3N) were purchased by TCI. The commercial polydimethylsiloxane film (PDMS) was purchased from Shanghai Onway Technology Co., Ltd. The silicon wafers were purchased from Suzhou Research Materials Microtech Co., Ltd.

Device fabrication and characterization. h-BN flakes and MoS_2 flakes were mechanically exfoliated by the Scotch-tape method, transferred to PDMS, and then

transferred on the oxidized silicon substrate (t_{ox} = 285 nm). The thickness of flakes was monitored by an optical microscope and confirmed by Raman spectroscopy and Atomic Force Microscopy (AFM). MoS_2 FETs were fabricated by direct-write lithography and Au electrodes (40nm) by thermal evaporation. The lift-off process was carried out in acetone. The as-fabricated devices were annealed for 30 minutes in a mixture of hydrogen (5%) and argon (95%) to improve the devices' performance. The *N*-benzylmaleimide and triethylamine were added to the ACN. The MoS_2 FETs reacted in the mixture overnight at the glovebox. All the devices were electrically characterized in a Lake shore probe station connected to a Keithley 4200. The Raman and PL spectra of MoS_2 were acquired with a Renishaw InVia spectrometer equipped with a 532nm laser.

The Calculation of Carrier Density. The pristine carrier density in 2D materials n_{2D} can be calculated based on the following equation:

$$n_{2D} = \frac{\sigma_{2D}}{q\mu} = \frac{I_d L}{V_d W q \mu}$$

where the σ_{2D} is the conductivity of the 2D materials, q is the elementary charge, L and W are the channel length and width, and μ is carrier mobility. Therefore, the functionalization with N-benzylmaleimide (Nbm) induced charge density could be extracted by $\Delta n = C_i \frac{\Delta V_{th}}{q}$, where the ΔV_{th} is the variation induced by Nbm, C_i is the capacitance of dielectric per unit area.

The Calculation of Carrier Mobility. The carrier mobility μ was determined by $\mu = \frac{dI_d}{dV_g} \times \frac{L}{W C_i V_d}$.

The Calculation of Schottky barriers. We extracted the Schottky barriers by using the thermionic emission equation $I_d = AA_{2D}^{*}T^{\frac{3}{2}}\exp\left[-\frac{q}{k_BT}\left(\Phi_B - \frac{V_d}{n}\right)\right]$, where A is contact area of junction, A_{2D}^{*} is the two-dimensional equivalent Richardson constant, q is the magnitude of the electron charge, Φ_B is the Schottky barrier height, k_B is the Boltzmann constant, n is the ideality factor, and V_d is the drain-source bias.[24,26]

The Arrehenius polt (ln $(I_d/T^{3/2})$ vs $1000/T$ curves for various V_g) was plotted and the slope (S) is subsequently plotted as a function of V_g. In this way, the Φ_B under various gate voltages and the effective Φ_B (under the flat-band condition) can be obtained.

Theoretical calculations. Density functional theory (DFT) calculations were performed using the generalized gradient approximation for the exchange-correlation potential, the projector augmented wave method[29] and a plane-wave basis set as implemented in the Vienna ab-initio simulation package (VASP)[30]. Dispersion correction was made at the van der Waals density functional (vdW-DF)[31, 32] level, with the optB86b functional for the exchange potential (optB86b-vdW)[32, 33], which was proved to be accurate in describing the structural properties of layered materials[34, 35]. A 3×3 supercell of MoS_2 and a vacuum layer of around 16 Å were adopted in calculations. The kinetic energy cut-off for the plane-wave basis was set to 500 eV. A 7×7×1 *k*-mesh and a Gaussian smearing with sigma of 0.01 eV were used for geometric properties optimization and electronic structure calculations. In structural relaxations, all atoms were fully relaxed until the residual force on every atom was less than 0.02 eV/Å.

ASSOCIATED CONTENT

Supporting Information

The Supporting Information is available free of charge on the ACS Publications website at DOI: xxxxx.

Figure S1-S6, S10 and S12-S17: Materials and electrical characterization of MoS_2 FETs (pristine and Nbm-MoS_2) dependent on the concentrations of *N*-benzylmaleimide, the annealing temperature, and the selected substrates. Figure S7-S9 and S18: Atomic configurations of Nbm-MoS_2 considered in DFT calculations, electronic structures of 3×3 MoS_2 supercell, and spatial structure of wavefunction norms for the six bands below the Nbm-HOMO. Figure S11: AFM and Raman spectra of the three-layer Nbm-MoS_2 flake.

AUTHOR INFORMATION

Corresponding Author

*E-mail: zhangxiaowei@nbu.edu.cn, qiaojs@bit.edu.cn, samori@unistra.fr, yudazhao@zju.edu.cn

Author Contributions

#J.M. and L.W. contributed equally to this work. Y.Z. and P. S. conceived the experiment. J.M. performed the AFM study, spectroscopic characterization and carried out the device fabrication and characterization with the help of Z. B., Q. Z., T. Z., X. P., J. H., X. Y., B. Y., and X. Z.. L.W. performed the DFT calculation under the supervision

of J. Q and W. J.. J. M. and Y.Z. co-wrote the paper. All authors discussed the results and contributed to the interpretation of data as well as to editing the manuscript.

Notes

The authors declare no competing interests.

ACKNOWLEDGMENTS

We thank ZJU Micro-Nano Fabrication Center and ZJU-Hangzhou International Innovation Center for the supports. We thank Dr. Zhihao Gong, Prof. Hua Wang, Mr. Yuyang Wu, and Prof. Renchao Che for the valuable discussion. The project was primarily supported by the National Natural Science Foundation of China (62090030, 62090034, 62104214, 92164106, 61874094, 11674053), the Young Elite Scientists Sponsorship Program by CAST (2021QNRC001), the Opening Project of Key Laboratory of Optoelectronic Chemical Materials and Devices of Ministry of Education, Jianghan University, Kun-Peng Program of Zhejiang Province, and the National Key R&D Program of China (2018YFA0307300). We acknowledge funding also from the European Commission through the ERC project SUPRA2DMAT (GA-833707), the Graphene Flagship Core 3 project (GA-881603) and the Institut Universitaire de France (IUF). L.W. was supported by the Outstanding Innovative Talents Cultivation Funded Programs 2022 of Renmin University of China.

Reference

1. Allain, A.; Kang, J.; Banerjee, K.; Kis, A. Electrical Contacts to Two-Dimensional

Semiconductors. *Nat. Mater.* **2015,** *14* (12), 1195-1205.

2. Xu, Y.; Cheng, C.; Du, S.; Yang, J.; Yu, B.; Luo, J.; Yin, W.; Li, E.; Dong, S.; Ye, P.; Duan, X. Contacts between Two- and Three-Dimensional Materials: Ohmic, Schottky, and P–N Heterojunctions. *ACS Nano* **2016,** *10* (5), 4895-4919.

3. Zhao, Y.; Xu, K.; Pan, F.; Zhou, C.; Zhou, F.; Chai, Y. Doping, Contact and Interface Engineering of Two-Dimensional Layered Transition Metal Dichalcogenides Transistors. *Adv. Funct. Mater.* **2017,** *27* (19), 1603484.

4. Liu, Y.; Guo, J.; Zhu, E.; Liao, L.; Lee, S.-J.; Ding, M.; Shakir, I.; Gambin, V.; Huang, Y.; Duan, X. Approaching the Schottky–Mott Limit in Van Der Waals Metal–Semiconductor Junctions. *Nature* **2018,** *557* (7707), 696-700.

5. Shen, P.-C.; Su, C.; Lin, Y.; Chou, A.-S.; Cheng, C.-C.; Park, J.-H.; Chiu, M.-H.; Lu, A.-Y.; Tang, H.-L.; Tavakoli, M. M.; Pitner, G.; Ji, X.; Cai, Z.; Mao, N.; Wang, J.; Tung, V.; Li, J.; Bokor, J.; Zettl, A.; Wu, C.-I.*, et al.* Ultralow Contact Resistance Between Semimetal and Monolayer Semiconductors. *Nature* **2021,** *593* (7858), 211-217.

6. Cho, K.; Pak, J.; Kim, J.-K.; Kang, K.; Kim, T.-Y.; Shin, J.; Choi, B. Y.; Chung, S.; Lee, T. Contact-Engineered Electrical Properties of MoS_2 Field-Effect Transistors via Selectively Deposited Thiol-Molecules. *Adv. Mater.* **2018,** *30* (18), 1705540.

7. Kiriya, D.; Tosun, M.; Zhao, P.; Kang, J. S.; Javey, A. Air-Stable Surface Charge Transfer Doping of MoS_2 by Benzyl Viologen. *J. Am. Chem. Soc.* **2014,** *136* (22), 7853-7856.

8. Yue, D.; Kim, C.; Lee, K. Y.; Yoo, W. J. Ohmic Contact in 2D Semiconductors via

the Formation of a Benzyl Viologen Interlayer. *Adv. Funct. Mater.* **2019,** *29* (7), 1807338.

9. Fang, H.; Chuang, S.; Chang, T. C.; Takei, K.; Takahashi, T.; Javey, A. High-Performance Single Layered WSe_2 P-FETs with Chemically Doped Contacts. *Nano Lett.* **2012,** *12* (7), 3788-3792.

10. Borah, A.; Nipane, A.; Choi, M. S.; Hone, J.; Teherani, J. T. Low-Resistance P-Type Ohmic Contacts to Ultrathin WSe_2 by Using a Monolayer Dopant. *ACS Appl. Electron. Mater.* **2021,** *3* (7), 2941-2947.

11. Vera-Hidalgo, M.; Giovanelli, E.; Navío, C.; Pérez, E. M. Mild Covalent Functionalization of Transition Metal Dichalcogenides with Maleimides: A "Click" Reaction for 2H-MoS_2 and WS_2. *J. Am. Chem. Soc.* **2019,** *141* (9), 3767-3771.

12. Kukucska, G.; Koltai, J. Theoretical Investigation of Strain and Doping on the Raman Spectra of Monolayer MoS_2. *Phys. Status Solidi B* **2017,** *254* (11), 1700184.

13. Mouri, S.; Miyauchi, Y.; Matsuda, K. Tunable Photoluminescence of Monolayer MoS_2 via Chemical Doping. *Nano Lett.* **2013,** *13* (12), 5944-5948.

14. Mak, K. F.; He, K.; Lee, C.; Lee, G. H.; Hone, J.; Heinz, T. F.; Shan, J. Tightly Bound Trions in Monolayer MoS_2. *Nat. Mater.* **2013,** *12* (3), 207-211.

15. Lee, G.-H.; Cui, X.; Kim, Y. D.; Arefe, G.; Zhang, X.; Lee, C.-H.; Ye, F.; Watanabe, K.; Taniguchi, T.; Kim, P.; Hone, J. Highly Stable, Dual-Gated MoS_2 Transistors Encapsulated by Hexagonal Boron Nitride with Gate-Controllable Contact, Resistance, and Threshold Voltage. *ACS Nano* **2015,** *9* (7), 7019-7026.

16. Lee, M.; Kim, Y.; Mohamed, A. Y.; Lee, H.-K.; Ihm, K.; Kim, D. H.; Park, T. J.;

Cho, D.-Y. Direct Evidence of Electronic Interaction at the Atomic-Layer-Deposited MoS_2 Monolayer/SiO_2 Interface. *ACS Appl. Mater. Interfaces* **2020,** *12* (48), 53852-53859.

17. Zhao, Y.; Gobbi, M.; Hueso, L. E.; Samorì, P. Molecular Approach to Engineer Two-Dimensional Devices for CMOS and Beyond-CMOS Applications. *Chem. Rev.* **2022,** *122* (1), 50-131.

18. Kang, J.; Liu, W.; Sarkar, D.; Jena, D.; Banerjee, K. Computational Study of Metal Contacts to Monolayer Transition-Metal Dichalcogenide Semiconductors. *Phys. Rev. X* **2014,** *4* (3), 031005.

19. Kim, C.; Moon, I.; Lee, D.; Choi, M. S.; Ahmed, F.; Nam, S.; Cho, Y.; Shin, H.-J.; Park, S.; Yoo, W. J. Fermi Level Pinning at Electrical Metal Contacts of Monolayer Molybdenum Dichalcogenides. *ACS Nano* **2017,** *11* (2), 1588-1596.

20. Radisavljevic, B.; Kis, A. Mobility Engineering and a Metal–Insulator Transition in Monolayer MoS_2. *Nat. Mater.* **2013,** *12* (9), 815-820.

21. Kaasbjerg, K.; Thygesen, K. S.; Jacobsen, K. W. Phonon-Limited Mobility in N-Type Single-Layer MoS_2 from First Principles. *Phys. Rev. B* **2012,** *85* (11), 115317.

22. Fivaz, R.; Mooser, E. Mobility of Charge Carriers in Semiconducting Layer Structures. *Phys. Rev.* **1967,** *163* (3), 743-755.

23. Liu, Y.; Wu, H.; Cheng, H.-C.; Yang, S.; Zhu, E.; He, Q.; Ding, M.; Li, D.; Guo, J.; Weiss, N. O.; Huang, Y.; Duan, X. Toward Barrier Free Contact to Molybdenum Disulfide Using Graphene Electrodes. *Nano Lett.* **2015,** *15* (5), 3030-3034.

24. Lee, S.; Tang, A.; Aloni, S.; Philip Wong, H. S. Statistical Study on the Schottky

Barrier Reduction of Tunneling Contacts to CVD Synthesized MoS_2. *Nano Lett.* **2016,** *16* (1), 276-281.

25. Das, S.; Chen, H.-Y.; Penumatcha, A. V.; Appenzeller, J. High Performance Multilayer MoS_2 Transistors with Scandium Contacts. *Nano Lett.* **2013,** *13* (1), 100-105.

26. Chen, J.-R.; Odenthal, P. M.; Swartz, A. G.; Floyd, G. C.; Wen, H.; Luo, K. Y.; Kawakami, R. K. Control of Schottky Barriers in Single Layer MoS_2 Transistors with Ferromagnetic Contacts. *Nano Lett.* **2013,** *13* (7), 3106-3110.

27. Cui, X.; Shih, E.-M.; Jauregui, L. A.; Chae, S. H.; Kim, Y. D.; Li, B.; Seo, D.; Pistunova, K.; Yin, J.; Park, J.-H.; Choi, H.-J.; Lee, Y. H.; Watanabe, K.; Taniguchi, T.; Kim, P.; Dean, C. R.; Hone, J. C. Low-Temperature Ohmic Contact to Monolayer MoS_2 by Van Der Waals Bonded Co/h-BN Electrodes. *Nano Lett.* **2017,** *17* (8), 4781-4786.

28. Wang, J.; Yao, Q.; Huang, C.-W.; Zou, X.; Liao, L.; Chen, S.; Fan, Z.; Zhang, K.; Wu, W.; Xiao, X.; Jiang, C.; Wu, W.-W. High Mobility MoS_2 Transistor with Low Schottky Barrier Contact by Using Atomic Thick h-BN As a Tunneling Layer. *Adv. Mater.* **2016,** *28* (37), 8302-8308.

29. Blöchl, P. E. Projector Augmented-Wave Method. *Phys. Rev. B* **1994,** *50* (24), 17953-17979.

30. Kresse, G.; Joubert, D. From Ultrasoft Pseudopotentials to the Projector Augmented-Wave Method. *Phys. Rev. B* **1999,** *59* (3), 1758-1775.

31. Dion, M.; Rydberg, H.; Schröder, E.; Langreth, D. C.; Lundqvist, B. I. Van Der Waals Density Functional for General Geometries. *Phys. Rev. Lett.* **2004,** *92* (24),

246401.

32. Lee, K.; Murray, É. D.; Kong, L.; Lundqvist, B. I.; Langreth, D. C. Higher-Accuracy Van Der Waals Density Functional. *Phys. Rev. B* **2010,** *82* (8), 081101.

33. Klimeš, J.; Bowler, D. R.; Michaelides, A. Van Der Waals Density Functionals Applied to Solids. *Phys. Rev. B* **2011,** *83* (19), 195131.

34. Hu, Z. X.; Kong, X.; Qiao, J.; Normand, B.; Ji, W. Interlayer Electronic Hybridization Leads to Exceptional Thickness-Dependent Vibrational Properties in Few-Layer Black Phosphorus. *Nanoscale* **2016,** *8* (5), 2740-50.

35. Zhao, Y.; Qiao, J.; Yu, P.; Hu, Z.; Lin, Z.; Lau, S. P.; Liu, Z.; Ji, W.; Chai, Y. Extraordinarily Strong Interlayer Interaction in 2D Layered PtS_2. *Adv. Mater.* **2016,** *28* (12), 2399-407.